Impurity scattering on the surface of topological-insulator thin films

Mahroo Shiranzaei,[1] Fariborz Parhizgar,[2,*] Jonas Fransson,[3] and Hosein Cheraghchi[1,†]
[1]*School of Physics, Damghan University, P.O. Box 36716-41167, Damghan, Iran*
[2]*School of Physics, Institute for Research in Fundamental Sciences (IPM), Tehran 19395-5531, Iran*
[3]*Department of Physics and Astronomy, Uppsala University, Box 516, SE-751 21 Uppsala, Sweden*
(Received 17 February 2017; revised manuscript received 24 May 2017; published 23 June 2017)

We address the electronic structure of the surface states of topological-insulator thin films with embedded local nonmagnetic and magnetic impurities. Using the T-matrix expansion of the real-space Green's function, we derive the local density of electron states and corresponding spin-resolved densities. We show that the effects of the impurities can be tuned by applying an electric field between the surface layers. The emerging magnetic states are expected to play an important role both in the ferromagnetic mechanism of magnetic topological insulators and in its transport properties. In the case of magnetic impurities, we have categorized the possible cases for different spin directions of the impurities as well as the spin direction in which the spin-resolved density of electron states is calculated and have related them to the spin susceptibility of the system.

DOI: 10.1103/PhysRevB.95.235429

I. INTRODUCTION

Topological insulators (TIs), a new state of materials with gapped bulk states and symmetry-protected gapless edge states, have recently attracted a great deal of attention in theoretical and experimental studies [1–7]. Historically, these gapless edge states, which arise from band inversion, were discovered first in two-dimensional (2D) TIs based on HgTe quantum wells [5,6]. Later, angle-resolved photoemission spectroscopy (ARPES) analysis of bismuth-based materials [8–12] revealed the presence of a single Dirac cone at the Γ point in the spectrum of the surface states, thus demonstrating the predictions also for three-dimensional (3D) TIs. These types of 3D TIs such as Bi_2Se_3 consist of layers interacting via van der Waals [7] interaction. Each layer, known as quintuple layer (QL), consists of Bi and Se atoms located in five surfaces, so that for thicknesses above 6 QLs, the bismuth-based material becomes a TI with gapless surface states [13].

The gapless surface states are topologically protected by time-reversal symmetry, which forbids backscattering from nonmagnetic impurities. In fact, owing to strong spin-orbit interaction in 3D TIs, spin-momentum locking of the surface states is the main theoretical reason for backscattering off impurities that break time-reversal symmetry [7,14].

In 3D TIs, numerous studies have tried to shed light on the effect of impurities [14–29]. However, because of some experimental contradictory results, scattering by magnetic and nonmagnetic impurities deposited on the surface of TIs is still a controversial topic and has an unclear picture. There are several explanations for describing enhanced experimental backscattering arising from different types of nonmagnetic impurities deposited on the surface of 3D TIs [14,27]. This enhanced backscattering is attributed to spatial distribution [23] and concentration of impurities and defects and also electron scattering by the step edges in the surface [27] of TI thin films.

On the other hand, bulk-doped magnetic impurities in 3D TIs give rise to a local gap around the Dirac cone [15,16,19–21] which is attributed to ferromagnetically ordered impurities, leading to a magnetic field-induced gap [15,30]. However, the gap opening in the Dirac cone cannot emerge at the stage of a single impurity, while its local density of states (LDOS) and spin LDOS will be remarkably changed [31]. Moreover, it was shown that the scattering and also transport properties of TIs depend on the polarization direction of the magnetic impurity [14,32]. The effect of Coulomb magnetic scatterers [18] and weak localization in the presence of nonmagnetic impurities were the subject of other researches too [17].

Although itinerant electrons in the surface of TIs are supposed to provide dissipationless transport due to the lack of backscattering, in practice, the bulk states also play a role in the transport properties [33] and make realization of the pure surface states hard. This problem also occurs when scattering by surface impurities is disturbed by scatterings coming from the bulk doping [12]. One way to reduce the effect of bulk states is to use thin slabs [34]. For TIs with a thickness of 5 QLs and thinner, the two surface states hybridize with each other, giving rise to a gap in the surface state's energy dispersion [13]. Such ultrathin TIs can be considered double-layer Rashba materials, which, according to their additional degree of freedom, can provide interesting features [35–37]. Also, the bilayerlike material opens the possibility to engineer the band structure of a TI thin film by applying an electric field perpendicular to the surfaces. Such a field (such a phenomenon can originate from the effect of the substrate) would separate the degenerate band dispersion like a Rashba splitting, as depicted in the Fig. 1(b). This extra electrical tunability of TI thin films makes them very favorable to use in topological magnetoelectric technology and also spintronic devices [38–42]. It was theoretically predicted that a topological transition from 2D quantum spin Hall (QSH) states to a normal insulator can be induced by an applied electric field V after a critical value [41,43–45]. Also it has been shown that a special form of tunneling between different surfaces together with the possibility of Rashba-type splitting can lead to topological superconductivity in these materials [46].

*fariborz.parhizgar@ipm.ir
†cheraghchi@du.ac.ir

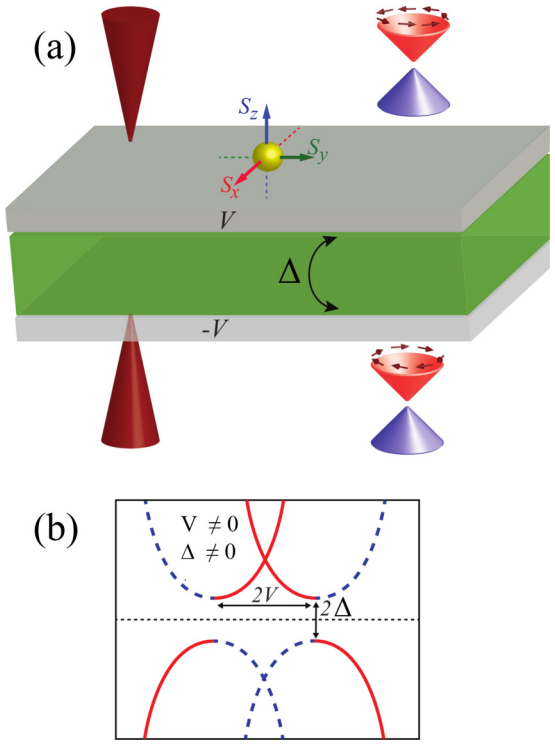

FIG. 1. (a) Schematic of a TI thin film (green area) with its surfaces (gray area), with opposite helical modes for different surfaces. Here, V shows the applied potential, and Δ is the hybridization between different surfaces. Red cones on the upper and lower surfaces illustrate STM tips that show the measurement can be done on both surfaces. A single impurity is illustrated as a yellow sphere which can be a nonmagnetic or magnetic impurity. In the case of the magnetic impurity, it can be aligned in one of the spin directions $\hat{x},\hat{y},\hat{z}$. (b) Schematic of band energy dispersion for the TI thin film, Eq. (4). Here, the blue dashed lines (the red solid lines) show the dispersion coming mostly from the upper (lower) surface.

The quantum anomalous Hall (QAH) effect, theoretically predicted in Ref. [47], was experimentally realized in magnetically doped TI thin films [48–50]. In fact, magnetic ordering in TI thin films leads to a band topology at zero external magnetic field. Although this effect has been confirmed by other experimental groups, the theoretical background, especially the mechanism generating such a ferromagnetism, is still under debate [26,47,51–57]. So investigation of the effect of impurity on the density of states in this material is very important. Since the QAH experiment has been done at zero chemical potential, the role of impurity bands in both transport properties and the mechanism of coupling between impurities is very important when the chemical potential lies inside the gap.

In this work, we show how a single impurity influences the band structure of a TI thin film. By using Green's function formalism and making a T-matrix expansion [15,23,31,58–61], we analytically explore the local density of electron states and spin LDOS near nonmagnetic and magnetic impurities, respectively, and show the emergence of new states in the spectrum due to the presence of these impurities. Since these new states can have an important effect on the transport properties, such as the QAH effect, we study their behavior as a function of the system parameters such as the type of impurity and its potential and also TI parameters like the electric potential difference and hybridization between surfaces. In addition, we indicate that one can electrically tune the effect of impurity on the LDOS and spin LDOS of the system and so manipulate the electronic and spin texture of the system by an applied electric potential.

The impurities in TIs can be located in the bulk as well as on the surface; however, since TIs usually should be in proximity to superconductors or ferromagnets for possible applications, locating the impurities on the surface provides more applications [14]. Hence, in this work we restrict ourselves to surface impurities. Also, we assume that the impurities are sufficiently diluted that multiple scatterings between impurities can be neglected, which allows us to restrict the study to the single-impurity picture.

The arrangement of this paper is as follows. First, in Sec. II, the effective model Hamiltonian of a 2D TI thin film is presented. We state how the Green's function of the system is calculated using the T-matrix approach and give the calculations of the LDOS and the spin LDOS in Sec. III. In Sec. IV, we focus on the obtained results in the case of (i) nonmagnetic and (ii) magnetic impurities and describe what happens in the LDOS. Moreover, for the sake of straightforwardness, we introduce a useful model named the *two-atom model* to describe some of our results. Finally, in Sec. V, the paper is briefly concluded and summarized. Furthermore, details of the calculations are provided in the appendixes.

II. MODEL HAMILTONIAN

As has been shown before, the low-energy physics of a topological insulator that occurs in the vicinity of the Γ point comes mostly from four p_z orbitals $|p_z^\tau,s\rangle$, where $\tau=\pm1$ shows even and odd parities and s refers to different spins [7,37,43]. For a thin slab of a TI with periodic boundary conditions in the $\hat{x}$ and $\hat{y}$ directions and finite width in the $\hat{z}$ direction, the Hamiltonian takes the form

$$H_{3D} = C - D_1\partial_z^2 + D_2k^2 + \begin{pmatrix} M(k)\sigma_z - iA_1\sigma_x\partial_z & A_2k_-\sigma_x \\ A_2k_+\sigma_x & M(k)\sigma_z + iA_1\sigma_x\partial_z \end{pmatrix}, \quad (1)$$

where $k_\pm = k_x \pm ik_y$; $k=\sqrt{k_x^2+k_y^2}$; $M(k) = M + B_1\partial_z^2 - B_2k^2$; $A_{1,2}, B_{1,2}, C$, and $D_{1,2}$ are coefficients; and M are model parameters that can be fixed by *ab initio* calculations. By solving the eigenvalue problem of the above Hamiltonian with vanishing eigenstates at the boundaries, $z=\pm d/2$, where d is the thickness of the TI, one can obtain an effective Hamiltonian model for a TI thin film around the Γ point as [13,35]

$$H_0(k) = -Dk^2\sigma_0\otimes\tau_0 + [\hbar v_F(\sigma\times\mathbf{k})\cdot\hat{z} + V\sigma_0]\otimes\tau_z + \Delta\sigma_0\otimes\tau_x, \quad (2)$$

where σ and τ denote the Pauli matrices in spin and surface spaces, respectively, D is a coefficient that represents the electron-hole asymmetry in the system, v_F is the Fermi velocity of the surface electrons, $\mathbf{k}$ denotes the wave vector ($k=|\mathbf{k}|$) of the surface electrons, and V is the potential difference between different surfaces. The last term, Δ,

TABLE I. Experimental parameters for the Bi_2Se_3 film [13].

QLs	v_F (10^5 m s^{-1})	Δ_0 (meV)	Δ_1 (eV Å^2)
3	4.81	69	18.0
4	4.48	35	10.0
5	4.53	2.05	5.0

represents hybridization between surface states, which in general is of the form $\Delta_0 - \Delta_1 k^2$ [see Fig. 1(a)]. While Δ_0 is a simple tunneling between different surfaces, Δ_1 may result in a quantum phase transition from a QSH insulator to a normal insulator for TI thin films whenever $\Delta_0\Delta_1 > 0$ and $V < \hbar v_F\sqrt{\Delta_0/\Delta_1}$ [41,45]. In this work, we restrict ourselves to the low-energy regime of the Hamiltonian and keep the terms up to linear order in k. The electron-hole asymmetry term D usually has a negligible effect on the electronic properties, while the effect of Δ_1 may be important for finite-size nanoribbons of a TI thin film where changes in the topology can result in the existence of zero-energy edge states [7,41,45]. Table I shows the experimental parameters of Bi_2Se_3, which have been achieved by fitting the parameters of Hamiltonian (2) with ARPES data [13].

In the basis of surface and spin spaces, the matrix form of the Hamiltonian can be expressed by

$$H_0(k) = \begin{bmatrix} V & i\hbar v_F k e^{-i\phi_k} & \Delta & 0 \\ -i\hbar v_F k e^{i\phi_k} & V & 0 & \Delta \\ \Delta & 0 & -V & -i\hbar v_F k e^{-i\phi_k} \\ 0 & \Delta & i\hbar v_F k e^{i\phi_k} & -V \end{bmatrix}, \tag{3}$$

where $\tan\phi_k = k_y/k_x$. The energy dispersion of this Hamiltonian is given by

$$E(k) = \pm\sqrt{(\hbar\, v_F\, k \mp V)^2 + \Delta^2}. \tag{4}$$

This dispersion relation is illustrated in Fig. 1(b). The structure inversion asymmetry (SIA) term, V, between the two surfaces can result from an interaction between the TI material and the substrate or an electric field applied perpendicular to the surface of the thin film [13]. The plots in Fig. 1(b) clearly demonstrate that the SIA generates a band splitting analogous to the Rashba splitting.

III. IMPURITY SCATTERING

The purpose of this section is to give a detailed account of the calculations of the impurity scattering and its effects on the local electronic structure. As we are interested in scattering of both nonmagnetic and magnetic impurities, we outline the general features of the calculations using a generic short-range scattering potential $\mathbf{U}(\mathbf{r}) = \mathbf{u}_{0/m}\delta(\mathbf{r} - \mathbf{r}_0)$. Then, we write the total Hamiltonian as

$$H = H_0(k) + \mathbf{U}(\mathbf{r}). \tag{5}$$

Specifically, from now on, we use the notation $\mathbf{u}_0 = u\sigma^0$ and $\mathbf{u}_m = \mathbf{m}\cdot\boldsymbol{\sigma}$ for the nonmagnetic and magnetic impurities, respectively, where σ^0 is the 2×2 identity matrix and $\boldsymbol{\sigma}$ is the vector of the Pauli matrices. Moreover, u provides the strength of the nonmagnetic scattering potential, and $\mathbf{m}$ represents both the strength of the magnetic scattering potential and the direction of the magnetic moment. In the present setup, we have assumed that the impurity is located on the upper surface; however, we are interested in its induced effects on both upper and lower surfaces.

The impurity-scattering-modified electronic structure is addressed by using real-space Green's functions (GFs) $\mathbf{G}(\varepsilon;\mathbf{r},\mathbf{r}')$, and we relate the LDOS $\rho(\mathbf{r},\varepsilon)$ and local magnetic texture (spin LDOS) $\boldsymbol{\rho}_\pm(\mathbf{r},\varepsilon)$ through the relations

$$\rho(\mathbf{r},\varepsilon) = -\frac{1}{\pi}\mathrm{Im\ Tr}\,\mathbf{G}(\varepsilon;\mathbf{r},\mathbf{r}), \tag{6a}$$

$$\boldsymbol{\rho}_\pm(\mathbf{r},\varepsilon) = -\frac{1}{2\pi}\mathrm{Im\ Tr}\,(\sigma^0 \pm \boldsymbol{\sigma})\mathbf{G}(\varepsilon;\mathbf{r},\mathbf{r}). \tag{6b}$$

Note that one can assume the magnetic impurity along one spin direction and calculate the spin LDOS in any other spin direction, which in experiment is equivalent to the spin-polarization direction of the scanning tunneling microscopy (STM) tip. In the above equation, $\boldsymbol{\sigma}$ shows the direction of the spin-LDOS measurement.

We consider the effects of impurity scattering by employing the T-matrix approach to calculate the modified, or dressed, GF [15,23,31,59,60,62–64]. Through a straightforward calculation, we have obtained the dressed GF (henceforth we set $r_0 = 0$),

$$\mathbf{G}^r(\varepsilon,\mathbf{r},\mathbf{r}') = \mathbf{G}_0^r(\varepsilon,\mathbf{r},\mathbf{r}') + \mathbf{G}_0^r(\varepsilon,\mathbf{r},0)\mathbf{T}(\varepsilon)\mathbf{G}_0^r(\varepsilon,0,\mathbf{r}'), \tag{7}$$

where G_0^r is the unperturbed (bare) retarded GF for the pristine material and the T matrix is defined by

$$\mathbf{T}(\varepsilon) = \mathbf{U} + \mathbf{U}\mathbf{G}_0^r(\varepsilon;0,0)\mathbf{T}(\varepsilon) = [\mathbf{U}^{-1} - \mathbf{G}_0^r(\varepsilon,0,0)]^{-1}. \tag{8}$$

This expression represents the propagation of an excitation in the perfect lattice in which scattering, to arbitrary order, takes place at the single impurity represented by $\mathbf{U}$ [65].

We relate the real-space GF to the reciprocal space properties through the Fourier transform ($\mathbf{R} = \mathbf{r} - \mathbf{r}'$)

$$\mathbf{G}_0^r(\varepsilon,\mathbf{R}) = \frac{1}{\Omega_{\mathrm{BZ}}}\int d\mathbf{k} e^{i\mathbf{k}\cdot\mathbf{R}}\mathbf{G}_0(\mathbf{k}), \tag{9}$$

where $\mathbf{G}_0(\varepsilon,\mathbf{k}) = [\varepsilon - H_0(\mathbf{k})]^{-1}$ and Ω_{BZ} shows the first Brillouin zone area.

In the following, we consider two different types of impurities separately, namely, nonmagnetic and magnetic impurities. First, we consider a local nonmagnetic impurity on the upper surface of the thin film for which $\mathbf{u}_0$ is a 4×4 matrix in the spin and surface spaces:

$$\mathbf{u_0} = u\delta(r)\begin{bmatrix} \sigma_0 & \vdots & 0 \\ \cdots & \cdots & \cdots \\ 0 & \vdots & 0 \end{bmatrix}. \tag{10}$$

Hence, for the nonmagnetic impurity we obtain the T matrix

$$\mathbf{T}_0 = \frac{u}{1-ug_{11}}\begin{bmatrix} \sigma_0 & \vdots & 0 \\ \cdots & \cdots & \cdots \\ 0 & \vdots & 0 \end{bmatrix}, \tag{11}$$

where

$$g_{11} = -\frac{2\pi}{\Omega_{\mathrm{BZ}}}\sum_{s=\pm}\int_0^{k_c} dkk\frac{a_s(\gamma+isV)}{\hbar^2 v_F^2 k^2-(V-is\gamma)^2} \tag{12}$$

is the top left component of $\mathbf{G}_0(\varepsilon,0,0)$ [see Eq. (A3)]. Here, k_c is the cutoff wave vector, $\gamma^2=\Delta^2-\varepsilon^2$, and $a_\pm=(\varepsilon/\gamma\pm i)/2$. Then, the corresponding LDOS is given by

$$\rho = \frac{-1}{\pi}\mathrm{Im}\left[2g_{11}-8\pi^2\alpha^2 u\frac{F_0-F_1}{1-ug_{11}}\right], \tag{13}$$

where $\alpha = 1/\hbar^2 v_F^2\Omega_{\mathrm{BZ}}$, $F_0=[\sum_{s=\pm} s\, a_{-s}(V+is\gamma)K_0^s]^2$, and $F_1=[\sum_{s=\pm} s a_{-s}K_1^s/\sqrt{-1/(V+is\gamma)^2}]^2$, whereas

$$K_0^s = K_0(-ir/x_s), \quad K_1^s = K_1(-ir/x_s), \tag{14}$$

in which $K_n(x)$ is the modified Bessel function and $x_s=\sqrt{\hbar^2v_F^2/(V\pm i\gamma)^2}$, $s=\pm1$.

In the case of a single magnetic impurity located on the upper surface of the thin film, the scattering potential is given by

$$\mathbf{u}_m = \delta(r)\begin{bmatrix} \mathbf{m}\cdot\boldsymbol{\sigma} & \vdots & 0 \\ \cdots & \cdots & \cdots \\ 0 & \vdots & 0 \end{bmatrix}. \tag{15}$$

For a magnetic moment polarized in the $\hat{\mathbf{z}}$ direction, $\mathbf{m}=m_z\hat{\mathbf{z}}$, the T matrix acquires the form

$$\mathbf{T}_m = \begin{bmatrix} \frac{m_z}{1-m_z g_{11}} & 0 & 0 & 0 \\ 0 & \frac{-m_z}{1+m_z g_{11}} & 0 & 0 \\ 0 & 0 & 0 & 0 \\ 0 & 0 & 0 & 0 \end{bmatrix}. \tag{16}$$

Hence, the corresponding spin LDOSs in the upper surface for the up and down spins are given by

$$\rho_\uparrow^{z,u} = \frac{-1}{\pi}\mathrm{Im}\left[g_{11}-4m^2\pi^2\alpha^2\left(\frac{F_0}{1-mg_{11}}-\frac{F_1}{1+mg_{11}}\right)\right], \tag{17a}$$

$$\rho_\downarrow^{z,u} = \frac{-1}{\pi}\mathrm{Im}\left[g_{11}+4m^2\pi^2\alpha^2\left(\frac{F_0}{1+mg_{11}}-\frac{F_1}{1-mg_{11}}\right)\right]. \tag{17b}$$

Analogous expressions are also obtained for the lower surface (see Appendix B 1). The same calculations can be simply done for other impurities' alignments and other spin directions' measurements.

IV. RESULTS

In this section, we present our results for the impurity scattering's influences on the surfaces of a TI thin film. We have not restricted our study to a single thickness and compare the results for 4 and 5 QLs of Bi_2Se_3. We study the impurity-scattering effects with respect to the potential drop V between the surfaces. In all our plots, we have calculated the LDOS and spin LDOS at a distance of 30 nm away from the scattering center.

A. Nonmagnetic impurity

We begin our survey by studying the effects arising from the nonmagnetic impurity. In Fig. 2, we plot the LDOS for the upper [Figs. 2(a) and 2(b)] and lower [Figs. 2(c) and 2(d)] surfaces for two different values of asymmetry potential, $V=0$ [Figs. 2(a) and 2(c)] and $V=50$ meV [Figs. 2(b) and 2(d)]. We have also included the LDOS for the unperturbed surfaces (dashed line) for reference. As expected, the hybridization between the surfaces creates a density gap whenever $|\varepsilon|<\Delta$ in the unperturbed LDOS. The density of states for the bare system related to Eq. (4) is given by $D(\varepsilon)=\sum_i \varepsilon k_i\Theta(\varepsilon^2-\Delta^2)/(\hbar v_F k_{cr}\pm V)$, where k_i refers to k points in which $\varepsilon=E(k)$ is given by $\hbar v_F k_i=\sqrt{\varepsilon^2-\Delta^2}\pm V$. It is obvious that the Van Hove singularities occur at $\hbar v_F k=\pm V$ for nonzero V and there is no Van Hove singularity at $V=0$. In the case with vanishing asymmetry potential, $V=0$, the LDOS grows linearly with energy outside the energy gap, and we notice that the electron-hole symmetry is preserved. However, under a finite asymmetry potential, the Van Hove singularities emerge at the band edges, and also the electron-hole symmetry breaks within the individual surface. Nevertheless, since the energy band dispersion is a combination of the properties from both surfaces, the overall electron-hole symmetry is preserved also for finite V. The LDOS in the lower surface is obtained by changing $\varepsilon\to-\varepsilon$ in the LDOS of the upper surface.

In the presence of a single nonmagnetic impurity, a single state emerges in the gap (see the in-gap peaks in the red solid lines in Fig. 2). This new peak is related to the poles of Eq. (13) (at $1-ug_{11}=0$) such that the position and height of this peak depend on the parameters of the system, e.g., u, Δ, V. By increasing the applied voltage, at low voltages, the peak shifts to higher energies. Therefore, there exists a way to control TI thin films as a semiconductor doped by acceptors or donors [66–68].

This shows that, in such a system, one is able to control and tune electrically the scattering effects of impurity. Furthermore, Van Hove singularities will be softened in the presence of nonmagnetic impurity, and in addition, the states outside the gap which were linear in terms of energy will change.

Also, one can see at $V=0$ [shown in Figs. 2(a) and 2(c)] that the upper surface has a stronger in-gap impurity peak in comparison to the lower surface; however, this order of their relative strengths may not hold for finite V. This suggests that, for a finite value of the asymmetry potential, one may see a stronger effect of impurity in the lower surface, although the impurity is located on the upper surface.

B. Magnetic impurity

Now we turn our attention to the effect of a magnetic impurity on the spin LDOS. The impurity's moment is aligned in the $\alpha(=\hat{x},\hat{y},\hat{z})$ direction, and the spin LDOS can be measured in an arbitrary $\beta(=\hat{x},\hat{y},\hat{z})$ direction of spin which

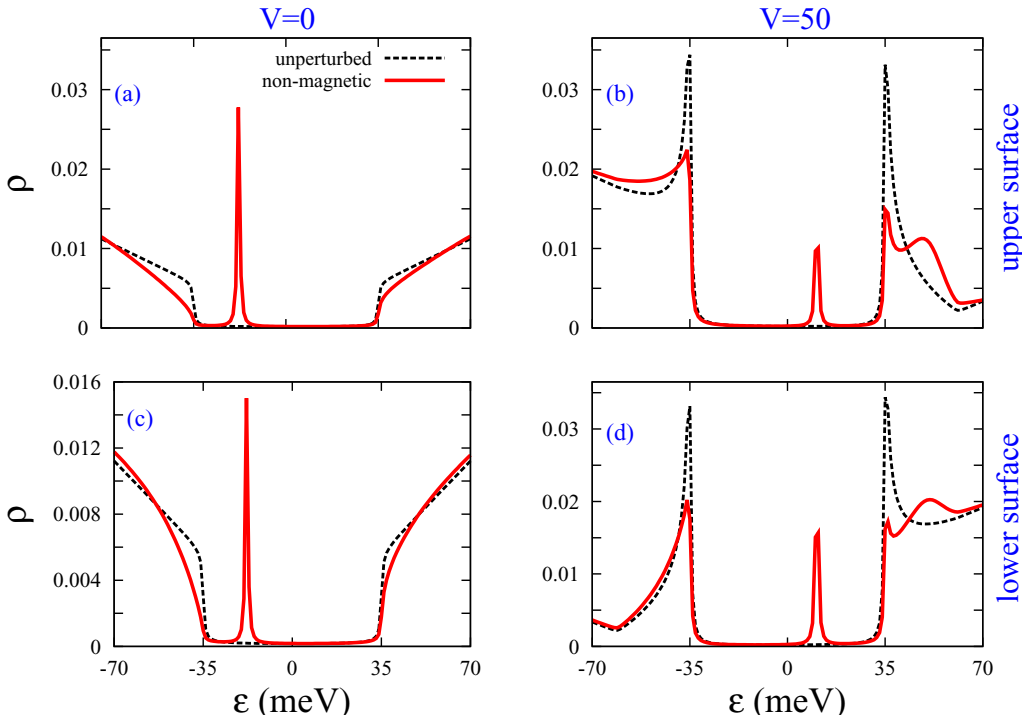

FIG. 2. The LDOS of the (a) and (b) upper and (c) and (d) lower surfaces for $\Delta = 35\,\text{meV}$, $u = 100\,\text{eV}$, $r = 30\,\text{nm}$, and different values of voltage, (a) and (c) $V = 0$ and (b) and (d) $V = 50\,\text{meV}$. The LDOS of the unperturbed surface (dashed line) is included for reference.

has been denoted in Eq. (6b) by $\boldsymbol{\sigma}$. Also, in general, this measurement depends on the distance vector $\mathbf{r}$, given the position of measurement from the impurity located at $r_0 = 0$. In this work, we have fixed the magnitude of the distance $r = 30\,\text{nm}$, and we have considered two different directions for $\mathbf{r}$, namely, $\hat{\mathbf{x}}$ and $\hat{\mathbf{y}}$. For simplicity, we denote such a situation by $\mathcal{F}^{\hat{\mathbf{x}}/\hat{\mathbf{y}}}_{\alpha,\beta}$.

Let us first focus on the cases of a $\hat{\mathbf{z}}$-polarized magnetic impurity [see Eq. (17)] and also assume the measurement is done in the $\hat{z}$ spin direction. The measurement of spin LDOS in this situation is independent of the $\mathbf{r}$ direction, so it can be labeled by $\mathcal{F}_{z,z}$. Figure 3 shows the spin LDOS of both the upper and lower surfaces for a 4-QL Bi_2Se_3 TI thin film in the situation $\mathcal{F}_{z,z}$. The gap parameter according to Table I is 35 meV, and two different asymmetry potentials, $V = 0$, 20 meV, have been compared. As the magnetic impurity breaks the degeneracy of spin states, two peaks appear inside the gap region. Roughly speaking, one can say each of these states should belong to one spin; however, since a TI thin film has a strong Rashba spin-orbit coupling which couples different spins, we would have four peaks at two energies.

For $V = 0$, the four peaks appearing in Figs. 3(a) and 3(c) have the symmetry that any spin LDOS, including the peaks in the positive energies, is equivalent to the opposite spin in the negative energy. For the lower surface at $V = 0$, shown by Fig. 3(c), just two peaks emerge according to different spins, and there would be no state for opposite spin there. This is the same for other thicknesses at $V = 0$. As one increases the potential V, both new states inside the gap shift to higher energies [Figs. 3(b) and 3(d)]. However, as it will be shown in Fig. 5, at higher voltages impurity states emerge at lower energies. For the lower surface [Fig. 3(d)], the four peaks come back, and they occur exactly at the same energies as on the upper surface. Also by increasing V the symmetry between different spins and energies breaks for both surfaces.

Analogy with two-atom model

To describe our results, we want to make an analogy of our system with a molecule model containing of two single atoms [69] (A and B with one orbital per site) connected to each other by the hopping energy t. Let us consider on-site energies to be $E_A = -M$ and $E_B = M$.

The molecular energy eigenvalues of the system are at $E_\pm = \pm\sqrt{t^2 + M^2}$, while the corresponding eigenstates are obtained for the bonding state as $\psi_+ = \beta\phi_A + \alpha\phi_B$ and for the antibonding state as $\psi_- = \alpha\phi_A - \beta\phi_B$, where $\alpha = \sin\phi$, $\beta = \cos\phi$, and $\tan 2\phi = t/M$. An asymmetry of the on-site energies results in an asymmetry in the LDOS on bonding and antibonding states $E_\pm$,

$$\text{LDOS}(E, A) = \alpha^2\,\delta(E - E_+) + \beta^2\,\delta(E - E_-), \quad (18a)$$

$$\text{LDOS}(E, B) = \alpha^2\,\delta(E - E_-) + \beta^2\,\delta(E - E_+). \quad (18b)$$

In the limit of the large energy difference (ionic limit), $|\,t\,| \ll M$, coefficients are nearly approximated by $\alpha \approx t/2M$ and $\beta \approx 1 - 0.5(t/2M)^2$, which show that the peaks in the LDOS are more localized on the energies close to the on-site energies of the given atom.

In terms of the analogy of A and B sites, which represent spin up and down in our model, the magnetic impurity generates different energies of different spins which play the role of M in the two-atom model, while the Rashba spin-orbit coupling is represented by t. The two-atom model shows why there are four peaks related to the up and down

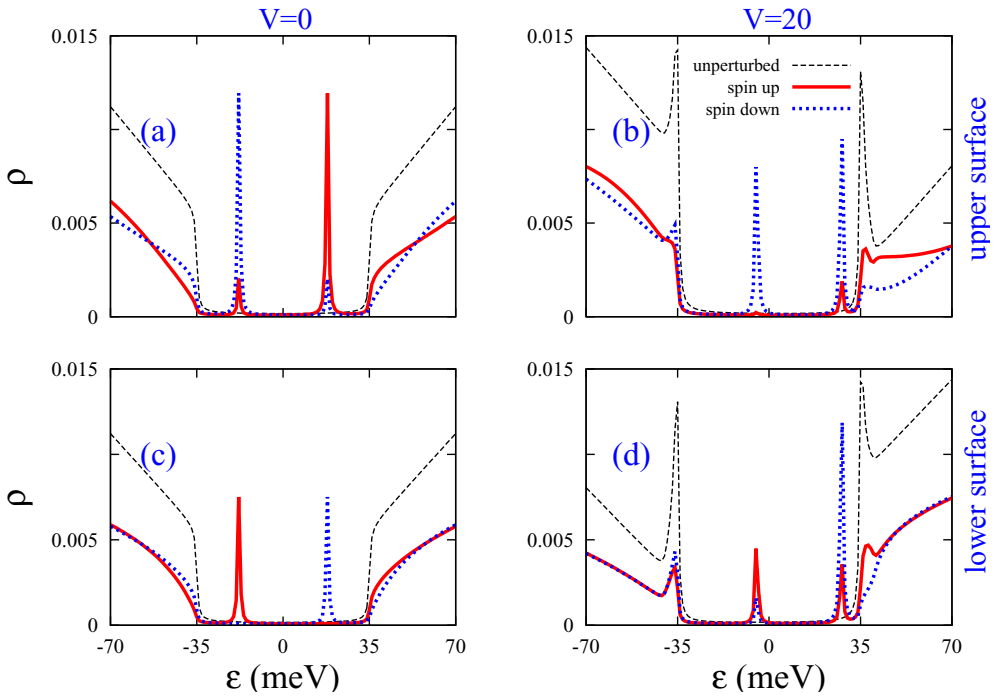

FIG. 3. The effect of a $\hat{\mathbf{z}}$-polarized magnetic impurity located on the upper surface of a TI thin film on the spin LDOS of upper or lower surface for $\Delta = 35\,\text{meV}$, $m = 100\,\text{eV}$, $r = 30\,\text{nm}$, and different values of voltage, $V = 0$, $20\,\text{meV}$. Dashed line refers to the LDOS of the unperturbed system. The red solid line and blue dotted line show spin-up and -down LDOSs, respectively.

spins at the bonding and antibonding energies. At $V = 0$ [Figs. 3(a) and 3(c)], there is no on-site energy on either surface; hence, the impurity states inside the gap can act like individual atoms, which leads to the new peaks inside the gap which are symmetrically distributed around the Fermi level at the energies $\pm E$. Also, consistent with our two-atom model, the LDOS for the spin-up (-down) peak at the bonding (antibonding) energy equals the LDOS of opposite spin at

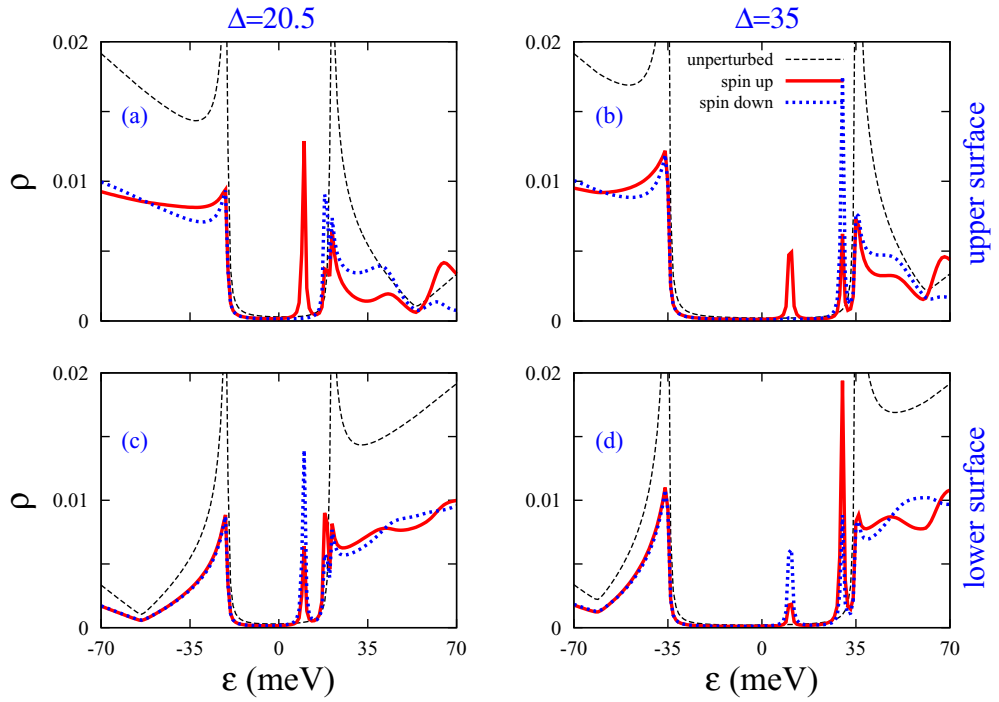

FIG. 4. The effect of the $\hat{\mathbf{z}}$-polarized magnetic impurity located on the upper surface of a TI thin film on the spin LDOS of the upper or lower surface for $\Delta = 20.5, 35\,\text{meV}$, $m = 100\,\text{eV}$, $r = 30\,\text{nm}$, and $V = 50\,\text{meV}$. Dashed line refers to the LDOS of the unperturbed system. The red solid line and blue dotted line show spin-up and -down LDOSs, respectively.

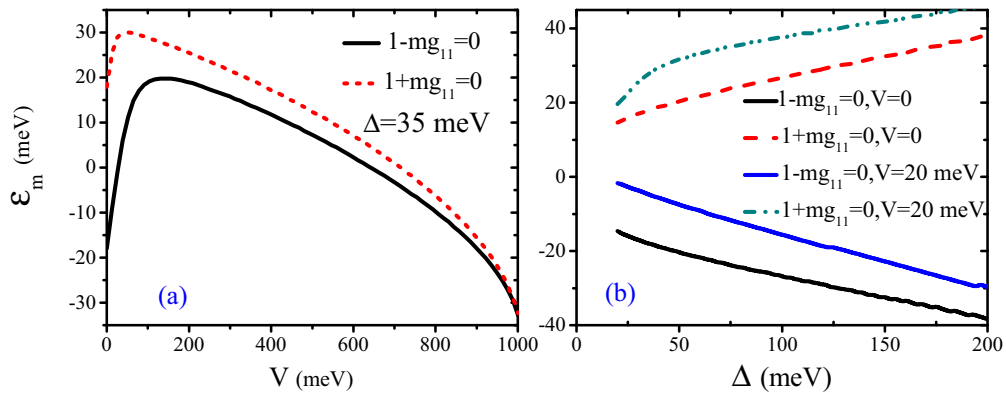

FIG. 5. The energy of the bound state induced by a single magnetic impurity inside the gap, with respect to (a) biased potential V and (b) gap size Δ.

the opposite energy. An increase in the magnetic moment of impurity leads to an enhanced spin LDOS on the bonding (antibonding) energy for spin up (down). Furthermore, in comparison with the upper surface, the up and down spin-polarized impurity states inside the gap are interchanged with each other in the lower surface as an effect of the negative Rashba coupling in the Hamiltonian at this surface [Fig. 3(c)]. As we increase the biased potential V, the on-site energies attributed to the upper and lower surfaces are asymmetric, which may cause an asymmetry in the LDOS and a shift in the bonding and antibonding energies. Based on the two-atom model, as long as the impurity states are localized in the gap, the spin-down LDOS on the antibonding state is enhanced in the upper surface, while the spin-up LDOS on the bonding state is enhanced in the lower surface. By further increasing V, the impurity states move toward each other and mix with states of the bare system electrons outside the gap where the two-atom model is no longer valid.

To investigate the effect of Δ on the spin LDOS, we depict the spin LDOS for 3- and 4-QL Bi_2Se_3 TI thin films at $V = 50$ meV in Fig. 4. As in Fig. 3, we assume the impurity is again $\hat{z}$ polarized and calculate the spin LDOS in the same spin direction, i.e., the $\mathcal{F}_{z,z}$ situation. First, by comparing Figs. 4(b) and 4(d) with Fig. 3, which are all for 4-QL Bi_2Se_3, it is observed that by increasing V to values higher than Δ in Fig. 4, the peaks shift to the band edges, giving rise to hybridization of the magnetic localized states with the TI states. This hybridization causes some distortions to occur in the conduction band.

Also a comparison between 3 and 4 QLs in Fig. 4 shows that by reducing Δ, the energy positions of the two peaks get closer to each other [31]. In addition, it is worth mentioning that the position and LDOS value of these new states inside the gap depend on the value of m. For very low magnetic strength, no peak will pop up inside the gap; as one increases this value, the peaks will appear, their LDOS value will increase by m, and they get close to each other. In the magnetic-impurity case, it should be noted that we have not considered any scattering of the electrostatic potential $\mathbf{u}_0$, so at $m \to 0$, there is no impurity state. In a real situation in which the magnetic impurity could generate a nonmagnetic potential as well, one should consider the general form of the potential $\mathbf{u}_0 + \mathbf{u}_m$ [60].

Figure 5 shows the bound-state energies of the magnetic impurity ε_m with respect to the biased voltage V and size of the gap Δ. These energies are related to the zeros of the denominator of the T matrix in Eqs. (17a) and (17b) in which $1 \pm mg_{11} = 0$. The behavior of the energy position according to the nonmagnetic impurity is equivalent to the ε_{m-} in which $1 - mg_{11} = 0$. In Fig. 5(a), where we depict ε_m with respect to V, two peaks start from symmetric energies at $V = 0$ (i.e., $|\varepsilon_{m-}| = |\varepsilon_{m+}|$), and they increase with respect to V. Increasing the biased voltage further causes both of these peaks' energies to decrease and reach negative energies and touch the valence band edge at a critical voltage (here $\sim$1 eV). After this critical voltage there is no impurity bound state inside the gap. Figure 5(b) depicts the bound state's energy with respect to the size of the gap from 20 up to 200 meV and for two different voltages, 0 and 20 meV. As one can see, at $V = 0$, the peaks occur at the symmetric energies with respect to the zero energy; however, both energies shift to higher values for $V = 20$ meV.

Furthermore, we consider the $\hat{\mathbf{x}}$-polarized magnetic impurity to be located on the upper surface and calculate the spin LDOS in the same spin direction. In this case, the results would be spatially anisotropic, so we have presented our result for two different spatial directions, $\hat{x}$ and $\hat{y}$; such situations are shown by $\mathcal{F}^{\hat{\mathbf{x}}/\hat{\mathbf{y}}}_{x,x}$ (see Appendix B 2). We present the effect of the $\hat{\mathbf{x}}$-polarized magnetic impurity in Fig. 6, which shows the spin LDOS of the thin film for both surfaces. Here, we choose tunneling $\Delta = 35$ meV and asymmetry potential $V = 50$ meV. The anisotropy of the spin LDOS for different spatial directions is visible. Comparing Figs. 3(b) and 3(d) with Figs. 6(a) and 6(c) clarifies that the spin LDOSs due to the situations $\mathcal{F}_{z,z}$ and $\mathcal{F}^{\hat{\mathbf{x}}}_{x,x}$ give us the same results. In addition, our calculations show the equality of the spin LDOS results of two situations, $\mathcal{F}^{\hat{\mathbf{x}}}_{x,x}$ and $\mathcal{F}^{\hat{\mathbf{y}}}_{y,y}$. Two other situations, $\mathcal{F}^{\hat{\mathbf{y}}}_{x,x}$ and $\mathcal{F}^{\hat{\mathbf{x}}}_{y,y}$, also result in the same spin LDOS. This can be described by the symmetry of the Hamiltonian where the Rashba term couples the electron's momentum to its spin, so any rotation applied to both spin and spatial directions will not change any physical quantity.

Figure 7 shows some of our findings when the direction of the polarization of the magnetic impurity is not the same as the spin direction of the spin LDOS. Here, $\Delta = 35$ meV,

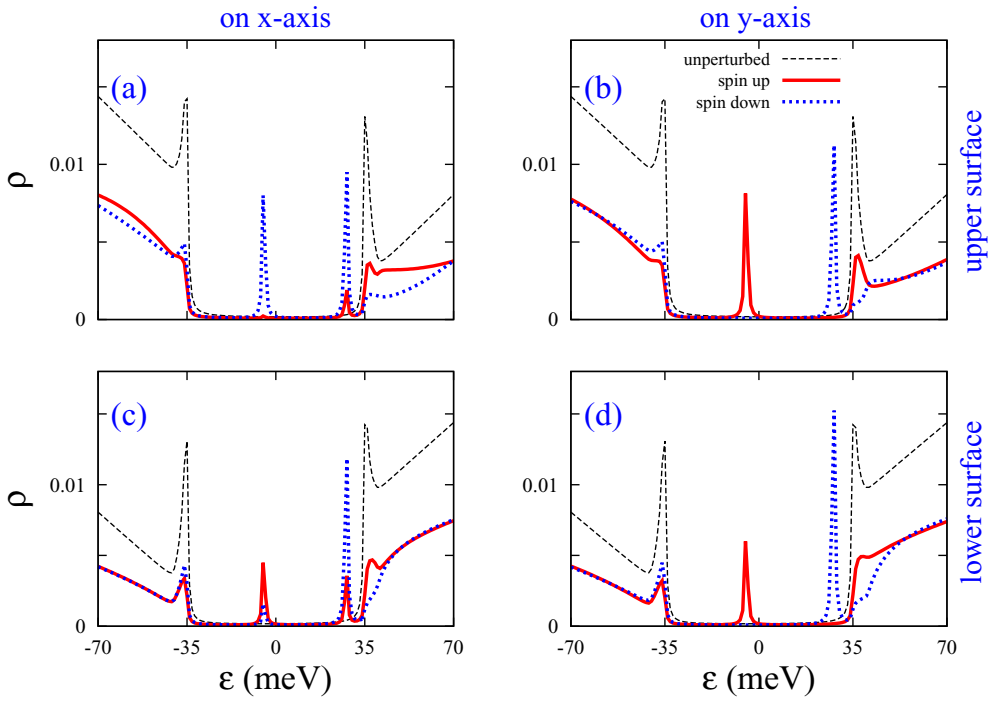

FIG. 6. The effect of the $\hat{\mathbf{x}}$-polarized magnetic impurity located on the upper surface of a TI thin film on the spin LDOS of the upper or lower surface on the $\hat{x}/\hat{y}$ axis. $\Delta = 35\,\text{meV}$, $V = 20\,\text{meV}$, $m = 100\,\text{eV}$, and $r = 30\,\text{nm}$. The dashed line refers to the LDOS of the unperturbed system. The red solid line and blue dotted line show spin-up and -down LDOSs, respectively.

$V = 20\,\text{meV}$, $m = 100\,\text{eV}$, and $r = 30$ nm. Figure 7(a) belongs to the $\mathcal{F}^{\hat{\mathbf{x}}}_{x,y}$ situation. In addition, Fig. 7(c) is obtained for the spin LDOS related to $\mathcal{F}^{\hat{\mathbf{x}}}_{y,x}$. These two plots suggest that their behaviors in the two situations are the same and that both situations lead to equal spin-up and -down LDOSs. This spin-unpolarized result would lead to zero spin susceptibility and, equivalently, Ruderman-Kittle-Kasuya-Yosida (RKKY) interaction [19] in the related directions since this interaction

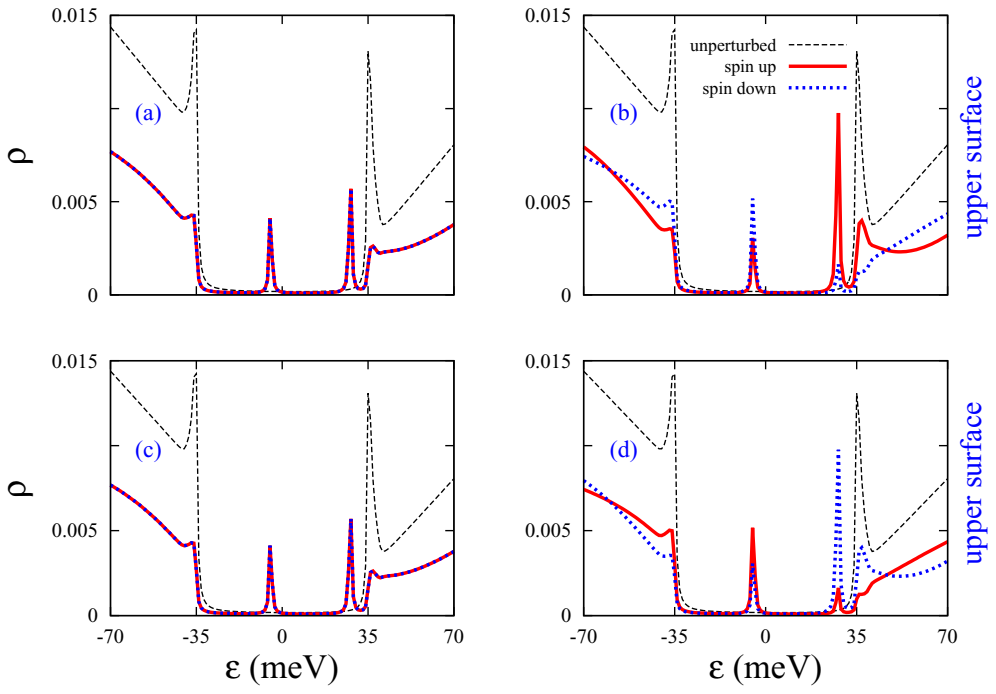

FIG. 7. The effect of different direction-polarized magnetic impurities located on the upper surface of a TI thin film on the various directional spin LDOSs of the upper surface on the $\hat{x}$ axis. Here, we chose $\Delta = 35\,\text{meV}$, $V = 20\,\text{meV}$, $m = 100\,\text{eV}$, and $r = 30\,\text{nm}$. The dashed line refers to the LDOS of the unperturbed system. The red solid line and blue dotted line show spin-up and -down LDOSs, respectively.

TABLE II. All the possible situations for magnetic impurity and calculated spin LDOS.

Cases under study	Related figures
$\mathcal{F}_{z,z}$, $\mathcal{F}^{\hat{x}}_{x,x}$, $\mathcal{F}^{\hat{y}}_{y,y}$	Figs. 3(b), 5(a)
$\mathcal{F}^{\hat{y}}_{x,x}$, $\mathcal{F}^{\hat{x}}_{y,y}$	Fig. 5(b)
$\mathcal{F}^{\hat{x}}_{x,y}$, $\mathcal{F}^{\hat{y}}_{x,y}$, $\mathcal{F}^{\hat{x}}_{y,x}$, $\mathcal{F}^{\hat{y}}_{y,x}$, $\mathcal{F}^{\hat{x}}_{y,z}$, $\mathcal{F}^{\hat{y}}_{x,z}$, $\mathcal{F}_{z,y}$	Figs. 6(a), 6(c)
$\mathcal{F}^{\hat{x}}_{x,z}$, $\mathcal{F}^{\hat{y}}_{y,z}$	Fig. 6(b)
$\mathcal{F}_{z,x}$	Fig. 6(d)

comes from the spin-up/-down imbalance of itinerant electrons caused by the existence of magnetic impurity [70]. In addition, we calculate the spin LDOS related to the $\mathcal{F}^{\hat{\mathbf{x}}}_{y,z}$ and $\mathcal{F}_{z,y}$ situations (where in the latter case, symmetry around the z axis causes $\mathcal{F}_{z,\beta}$ to be independent of spatial directions), and no difference between the results of these four situations is seen. Figures 7(b) and 7(d) depict the behavior of the spin LDOS related to two cases $\mathcal{F}^{\hat{\mathbf{x}}}_{x,z}$ and $\mathcal{F}_{z,x}$, respectively. Obviously, comparing them demonstrates that their spin LDOSs will be similar provided that spin up (down) changes to spin down (up). Above all, our calculations prove that $\mathcal{F}^{\hat{\mathbf{y}}}_{y,z}$ is achieved by application of $\pi/2$ rotation on $\mathcal{F}^{\hat{\mathbf{x}}}_{x,z}$ around the z axis. Briefly, Table II shows all the possible situations for fixed V and Δ, where we have categorized all possible situations in five different groups.

V. CONCLUSION

In conclusion, we have investigated the effect of single nonmagnetic and magnetic impurities on the LDOS and spin LDOS of TI thin films, respectively. We found analytic results for the Green's function in real space, so one can extract the DOS of the system with favorable experimental parameters. We found that a sufficiently strong potential associated with the single impurity generates states inside the gap. Hence, for many impurities with different potentials one can expect the gap to be filled or, at least, strongly modified. Since interesting experiments such as the quantum anomalous Hall effect have been done at zero chemical potential, the existence of these new states could have an important effect on the coupling of magnetic impurities (in the QAH experiment) as well as transport properties.

The existence of these new states becomes more important when one considers their relaxation time. The relaxation time of the impurity states is proportional to the inverse of their self-energy, which in the first Born approximation is proportional to the bare density of states of the system. The appearance of these new peaks inside the gap indicates that they are stable, with relatively long lifetimes compared to bound states outside the gap of materials known as virtual bound states.

Furthermore, we discussed the symmetries of these new states and categorized them with respect to the spin direction of the magnetic impurity and the spin direction in which spin LDOS is calculated. In addition, since the band dispersion of a TI thin film would be affected by the application of an electric field perpendicular to the surface of the TI thin film, we showed how one can tune the effect of both magnetic and nonmagnetic impurities using this voltage.

ACKNOWLEDGMENTS

F.P. thanks A. Sabzalipour and M. Mashkoori for useful discussions, and M.S. acknowledges the Institute for Research in Fundamental Sciences for hospitality while the last parts of this paper were prepared. J.F. acknowledges support from Vetenskapsrådet. H.C. acknowledges the International Center for Theoretical Physics (ICTP) for hospitality and support in capacity of Regular Associate member of the center.

APPENDIX A: DETAILS OF THE GREEN'S FUNCTION

In this appendix, the details of the calculation are given more explicitly. Using the Fourier transformation, the unperturbed retarded GF in real space for the TI thin film will be achieved:

$$\mathbf{G}^r_0(\varepsilon,r)=\begin{bmatrix} G_{11} & -G_{21} & \vdots & G_{13} & -G_{23} \\ G_{21} & G_{11} & \vdots & G_{23} & G_{13} \\ \cdots & \cdots & \cdots & \cdots & \cdots \\ G_{13} & -G_{23} & \vdots & G_{33} & -G_{43} \\ G_{23} & G_{13} & \vdots & G_{43} & G_{33} \end{bmatrix}, \tag{A1}$$

where

$$G_{11}(\varepsilon,r)=-2\pi\alpha\sum_{s=\pm}a_{-s}(\gamma-isV)K^s_0, \tag{A2a}$$

$$G_{21}(\varepsilon,r)=-2\pi i\alpha\sum_{s=\pm}\frac{a_{-s}}{\sqrt{\frac{-1}{(V-is\gamma)^2}}}K^s_1, \tag{A2b}$$

$$G_{13}(\varepsilon,r)=\pi i\alpha\frac{\Delta}{\gamma}\sum_{s=\pm}s(V+is\gamma)K^s_0, \tag{A2c}$$

$$G_{23}(\varepsilon,r)=-\pi i\alpha\frac{\Delta}{\gamma}\sum_{s=\pm}\frac{s}{\sqrt{\frac{-1}{(V+is\gamma)^2}}}K^s_1, \tag{A2d}$$

$$G_{33}(\varepsilon,r)=-2\pi\alpha\sum_{s=\pm}a_s(\gamma-isV)K^s_0, \tag{A2e}$$

$$G_{43}(\varepsilon,r)=-2\pi i\alpha\sum_{s=\pm}\frac{sa_s}{\sqrt{\frac{-1}{(V+is\gamma)^2}}}K^s_1, \tag{A2f}$$

where $K^{\pm}_{0/1}$, γ, α, and $a_{\pm}$ are defined in the main text.

Also the unperturbed on-site GF, $G^r_0(\varepsilon,0,0)=\langle 0|G^r_0(\varepsilon)|0\rangle$, can be obtained with the same Fourier transformation, but this time we need to apply a cutoff on k in Eq. (12) [58,71]:

$$\mathbf{G}^r_0(\varepsilon,0,0)=\begin{bmatrix} g_{11} & 0 & \vdots & g_{13} & 0 \\ 0 & g_{11} & \vdots & 0 & g_{13} \\ \cdots & \cdots & \cdots & \cdots & \cdots \\ g_{13} & 0 & \vdots & g_{33} & 0 \\ 0 & g_{13} & \vdots & 0 & g_{33} \end{bmatrix}, \tag{A3}$$

where g_{ij} are defined as

$$g_{11} = -\frac{2\pi}{\Omega_{\rm BZ}} \sum_{s=\pm} \int_0^{k_c} dk\ k\ \frac{a_s(\gamma + isV)}{\hbar^2 v_F^2 k^2 - (V - is\gamma)^2}, \tag{A4a}$$

$$g_{13} = i\frac{\pi\Delta}{\gamma\ \Omega_{\rm BZ}} \sum_{s=\pm} \int_0^{k_c} dk\ k\ \frac{s\ (is\gamma + V)}{\hbar^2 v_F^2 k^2 - (V + is\gamma)^2}, \tag{A4b}$$

$$g_{33} = -\frac{2\pi}{\Omega_{\rm BZ}} \sum_{s=\pm} \int_0^{k_c} dk\ k\ \frac{a_{-s}(\gamma + isV)}{\hbar^2 v_F^2 k^2 + (isV + \gamma)^2}. \tag{A4c}$$

APPENDIX B: THE SPIN LDOS

1. The $\hat{z}$-polarized magnetic impurity

In the presence of the $\hat{\mathbf{z}}$-polarized magnetic impurity on the upper surface, the spin-LDOS relations for the lower surface are

$$\rho_{\uparrow}^{z,l} = g_{33} + \frac{\pi^2\alpha^2\Delta^2 m/\gamma^2}{1 - mg_{11}}\left[\sum_{s=\pm}(\gamma - isV)K_0^s\right]^2 + \frac{\pi^2\alpha^2\Delta^2 m/\gamma^2}{1 + mg_{11}}\left[\sum_{s=\pm} -\frac{s\ K_1^s}{\sqrt{\frac{1}{(\gamma - isV)^2}}}\right]^2, \tag{B1a}$$

$$\rho_{\uparrow}^{z,l} = g_{33} + \frac{\pi^2\alpha^2\Delta^2 m/\gamma^2}{1 + mg_{11}}\left[\sum_{s=\pm}(\gamma - isV)K_0^s\right]^2 + \frac{\pi^2\alpha^2\Delta^2 m/\gamma^2}{1 - mg_{11}}\left[\sum_{s=\pm} -\frac{s\ K_1^s}{\sqrt{\frac{1}{(\gamma - isV)^2}}}\right]^2. \tag{B1b}$$

2. The $\hat{x}$-polarized magnetic impurity

The relations of the spin LDOS on the x axis for the upper and lower surfaces are calculated for the case where the magnetic impurity in the direction of $\hat{\mathbf{x}}$ locates on the upper surface:

$$\rho_{\uparrow}^{x,u} = g_{11} - 4m^2\pi^2\alpha^2\left\{\frac{[(V - i\gamma)K_0^- a_+ - (V + i\gamma)K_0^+ a_-]^2}{1 - mg_{11}} + \frac{[(V - i\gamma)K_1^- a_+ + (V + i\gamma)K_1^+ a_-]^2}{1 + mg_{11}}\right\}, \tag{B2a}$$

$$\rho_{\downarrow}^{x,u} = g_{11} - 4m^2\pi^2\alpha^2\left\{\frac{[(V - i\gamma)K_0^- a_+ - (V + i\gamma)K_0^+ a_-]^2}{1 + mg_{11}} + \frac{[(V - i\gamma)K_1^- a_+ + (V + i\gamma)K_1^+ a_-]^2}{1 - mg_{11}}\right\}, \tag{B2b}$$

$$\rho_{\uparrow}^{x,l} = g_{33} - \frac{\pi^2\alpha^2\Delta^2 m}{\gamma^2}\left\{\frac{[(V - i\gamma)K_0^- - (V + i\gamma)K_0^+]^2}{1 - mg_{11}} + \frac{[(V - i\gamma)K_1^- + (V + i\gamma)K_1^+]^2}{1 + mg_{11}}\right\}, \tag{B2c}$$

$$\rho_{\downarrow}^{x,l} = g_{33} - \frac{\pi^2\alpha^2\Delta^2 m}{\gamma^2}\left\{\frac{[(V - i\gamma)K_0^- - (V + i\gamma)K_0^+]^2}{1 + mg_{11}} + \frac{[(V - i\gamma)K_1^- + (V + i\gamma)K_1^+]^2}{1 - mg_{11}}\right\}. \tag{B2d}$$

[1] C. L. Kane and E. J. Mele, Phys. Rev. Lett. **95**, 226801 (2005).
[2] B. A. Bernevig and S. C. Zhang, Phys. Rev. Lett. **96**, 106802 (2006).
[3] C. L. Kane and E. J. Mele, Phys. Rev. Lett. **95**, 146802 (2005).
[4] S. Murakami, Phys. Rev. Lett. **97**, 236805 (2006).
[5] B. A. Bernevig, T. L. Hughes, and S. C. Zhang, Science **314**, 1757 (2006).
[6] M. König, S. Wiedmann, Ch. Brüne, A. Roth, H. Buhmann, L. W. Molenkamp, X. L. Qi, and Sh. Ch. Zhang, Science **318**, 766 (2007).
[7] H. Zhang *et al.*, Nat. Phys. **5**, 438 (2009).
[8] L. Fu, C. L. Kane, and E. J. Mele, Phys. Rev. Lett. **98**, 106803 (2007).
[9] L. Fu and C. L. Kane, Phys. Rev. B **76**, 045302 (2007).
[10] D. Hsieh *et al.*, Nature (London) **452**, 970 (2008).
[11] Y. Xia *et al.*, Nat. Phys. **5**, 398 (2009).
[12] Y. L. Chen *et al.*, Science **325**, 178 (2009).
[13] Y. Zhang *et al.*, Nat. Phys. **6**, 584 (2010).
[14] P. Sessi, F. Reis, T. Bathon, K. A. Kokh, O. E. Tereshchenko, and M. Bode, Nat. Commun. **5**, 5349 (2014).
[15] Q. Liu, C.-X. Liu, C. Xu, X.-L. Qi, and S.-C. Zhang, Phys. Rev. Lett. **102**, 156603 (2009).
[16] Y. L. Chen *et al.*, Science **329**, 659 (2010).
[17] H. T. He, G. Wang, T. Zhang, I. K. Sou, G. K. Wong, J. N. Wang, H. Z. Lu, S. Q. Shen, and F. C. Zhang, Phys. Rev. Lett. **106**, 166805 (2011).
[18] L. A. Wray *et al.*, Nat. Phys. **7**, 32 (2011).
[19] J. J. Zhu, D. X. Yao, Sh. C. Zhang, and K. Chang, Phys. Rev. Lett. **106**, 097201 (2011).
[20] A. M. Black-Schaffer and A. V. Balatsky, Phys. Rev. B **85**, 121103(R) (2012).
[21] A. M. Black-Schaffer and A. V. Balatsky, Phys. Rev. B **86**, 115433 (2012).
[22] C.-H. Lee and C.-K. Yang, Phys. Rev. B **87**, 115306 (2013).

[23] J. Fransson, A. M. Black-Schaffer, and A. V. Balatsky, Phys. Rev. B **90**, 241409(R) (2014).
[24] H. Ochoa, Phys. Rev. B **92**, 081410(R) (2015).
[25] Y. Jiang, C. Song, Z. Li, M. Chen, R. L. Greene, K. He, L. Wang, X. Chen, X. Ma, and Q.-K. Xue, Phys. Rev. B **92**, 195418 (2015).
[26] T. R. F. Peixoto, H. Bentmann, S. Schreyeck, M. Winnerlein, Ch. Seibel, H. Maaß, M. Al-Baidhani, K. Treiber, S. Schatz, S. Grauer, Ch. Gould, K. Brunner, A. Ernst, L. W. Molenkamp, and F. Reinert, Phys. Rev. B **94**, 195140 (2016).
[27] S. Bauer and C. A. Bobisch, Nat. Commun. **7**, 11381 (2016).
[28] A. Zyuzin, M. Alidoust, and D. Loss, Phys. Rev. B **93**, 214502 (2016).
[29] I. V. Bobkova, A. M. Bobkov, A. A. Zyuzin, and M. Alidoust, Phys. Rev. B **94**, 134506 (2016).
[30] D. A. Abanin and D. A. Pesin, Phys. Rev. Lett. **106**, 136802 (2011).
[31] R. R. Biswas and A. V. Balatsky, Phys. Rev. B **81**, 233405 (2010).
[32] A. Sabzalipour, J. Abouie, and S. H. Abedinpour, J. Phys. Condens. Matter **27**, 115301 (2015).
[33] J. Zhang *et al.*, Phys. Rev. B **91**, 075431 (2015).
[34] K. Hoefer *et al.*, Proc. Natl. Acad. Sci. USA **111**, 14979 (2014).
[35] S. S. Pershoguba and V. M. Yakovenko, Phys. Rev. B **86**, 165404 (2012).
[36] F. Parhizgar and A. M. Black-Schaffer, Phys. Rev. B **90**, 184517 (2014).
[37] F. Parhizgar, A. G. Moghaddam, and R. Asgari, Phys. Rev. B **92**, 045429 (2015).
[38] I. Žutić, J. Fabian, and S. Das Sarma, Rev. Mod. Phys. **76**, 323 (2004).
[39] C. Nayak *et al.*, Rev. Mod. Phys. **80**, 1083 (2008).
[40] J. Moore, Nat. Phys. **5**, 378 (2009).
[41] W.-Y. Shan, H.-Z. Lu, and S.-Q. Shen, New J. Phys. **12**, 043048 (2010).
[42] T. Dietl and H. Ohno, Rev. Mod. Phys. **86**, 187 (2014).
[43] J. Linder, T. Yokoyama, and A. Sudbo, Phys. Rev. B **80**, 205401 (2009).
[44] C. X. Liu, H. J. Zhang, B. Yan, X.-L. Qi, T. Frauenheim, X. Dai, Z. Fang, and S.-C. Zhang, Phys. Rev. B **81**, 041307(R) (2010).
[45] J. Wang, B. Lian, and S.-C. Zhang, Phys. Rev. Lett. **115**, 036805 (2015).
[46] F. Parhizgar and A. M. Black-Schaffer, arXiv:1609.01038.
[47] R. Yu *et al.*, Science **329**, 61 (2010).
[48] C.-Z. Chang *et al.*, Science **340**, 167 (2013).
[49] X. Kou, S.-T. Guo, Y. Fan, L. Pan, M. Lang, Y. Jiang, Q. Shao, T. Nie, K. Murata, J. Tang, Y. Wang, L. He, T.-K. Lee, W.-L. Lee, and K. L. Wang, Phys. Rev. Lett. **113**, 137201 (2014).
[50] J. G. Checkelsky, R. Yoshimi, A. Tsukazaki, K. S. Takahashi, Y. Kozuka, J. Falson, M. Kawasaki, and Y. Tokura, Nat. Phys. **10**, 731 (2014).
[51] P. Larson and W. R. L. Lambrecht, Phys. Rev. B **78**, 195207 (2008).
[52] M. G. Vergniory, M. M. Otrokov, D. Thonig, M. Hoffmann, I. V. Maznichenko, M. Geilhufe, X. Zubizarreta, S. Ostanin, A. Marmodoro, J. Henk, W. Hergert, I. Mertig, E. V. Chulkov, and A. Ernst, Phys. Rev. B **89**, 165202 (2014).
[53] E. O. Lachman *et al.*, Sci. Adv. **1**, e1500740 (2015).
[54] M. Li, C.-Z. Chang, L. Wu, J. Tao, W. Zhao, M. H. W. Chan, J. S. Moodera, J. Li, and Y. Zhu, Phys. Rev. Lett. **114**, 146802 (2015).
[55] M. Ye *et al.*, Nat. Commun. **6**, 8913 (2015).
[56] S. Grauer, S. Schreyeck, M. Winnerlein, K. Brunner, C. Gould, and L. W. Molenkamp, Phys. Rev. B **92**, 201304(R) (2015).
[57] P. Sessi *et al.*, Nat. Commun. **7**, 12027 (2016).
[58] N. M. R. Peres, F. Guinea, and A. H. Castro Neto, Phys. Rev. B **73**, 125411 (2006).
[59] A. V. Balatsky, I. Vekhter, and J. X. Zhu, Rev. Mod. Phys. **78**, 373 (2006).
[60] A. M. Black-Schaffer, A. V. Balatsky, and J. Fransson, Phys. Rev. B **91**, 201411(R) (2015).
[61] Y. L. Zou, J. Song, Ch. Bai, and K. Chang, Phys. Rev. B **94**, 035431 (2016).
[62] J. Fransson and A. V. Balatsky, Phys. Rev. B **75**, 195337 (2007).
[63] J.-H. She, J. Fransson, A. R. Bishop, and A. V. Balatsky, Phys. Rev. Lett. **110**, 026802 (2013).
[64] J. Fransson, Phys. Rev. B **92**, 125405 (2015).
[65] A. Gonis, *Green Function for Ordered and Disordered Systems* (North-Holland, Amsterdam, 1992).
[66] Y. Guo and J. Robertson, Sci. Rep. **5**, 14165 (2015).
[67] X.-B. Li *et al.*, Sci. Rep. **5**, 10848 (2015).
[68] A. Ziletti, A. Carvalho, D. K. Campbell, D. F. Coker, and A. H. Castro Neto, Phys. Rev. Lett. **114**, 046801 (2015).
[69] H. Cheraghchi, Doctoral dissertation, Sharif University of Technology, Tehran, Iran, 2007.
[70] M. Shiranzaei, F. Parhizgar, and H. Cheraghchi, arXiv:1702.02307.
[71] Z. F. Wang, R. Xiang, Q. W. Shi, J. Yang, X. Wang, J. G. Hou, and J. Chen, Phys. Rev. B **74**, 125417 (2006).